Intramolecular Bonding and Charge Distributions in XO_4 (X = Si, P, S, Cl and Ge, As, Se, Br) Oxyanions from Topological Analyses of the Electron Density

Jean-François Boily

Institut für Mineralogie und Petrographie, Swiss Federal Institute of Technology (ETH) Zürich, Sonneggstrasse 5, CH-8092 Zürich, Switzerland

Received: December 19, 2001; In Final Form: March 11, 2002

Intramolecular X−O bonds and charge distributions in XO_4 (X = Si, P, S, Cl, and Ge, As, Se, Br) oxyanions were investigated with topological analyses of the electron density in the frameworks of the theories of atoms in molecules (AIM) and of the electron localization function (ELF). The optimized geometries and wave functions of all oxyanions were obtained at the B3LYP/6-311+G(3df) level. AIM analyses recover a significant concentration of electrons at (3,−1) bond critical points increasing from SiO_4^{4-} (0.12 au) to ClO_4^{1-} (0.37 au) and from GeO_4^{4-} (0.14 au) to BrO_4^{1-} (0.27 au). Perchlorate is the only oxyanion exhibiting true shared interactions in the sense of AIM with a large and negative Laplacian of the electron density at the bond critical point. All other oxyanions are intermediate to shared and closed-shell interactions with positive values of the Laplacian of the electron density. ELF analyses tend to support the conclusions of AIM by localizing disynaptic basins between 3rd row X atoms and O with electron populations ranging from 1.56*e* (SiO_4^{4-}) to 1.84*e* (ClO_4^{1-}). The X−O bonds are also shown to be of donor−acceptor type. Fourth row oxyanions have highly delocalized and small disynaptic basin populations ranging from 0.27*e* (AsO_4^{3-}) to 0.30*e* (BrO_4^{1-}) with GeO_4^{4-} as the only oxyanion without any formally defined disynaptic basin. The attractive forces in these oxyanions are thus mostly of electrostatic nature. All ELF disynaptic basins have strong cross-contributions with the lone pair monosynaptic valence basins of O. These latter basins contain about three electron pairs (6.12*e*) for ClO_4^{1-} to about four (7.99*e*) for GeO_4^{4-}. Finally, the Merz−Kollman scheme was used to determine point charges that can reproduce the electrostatic potential of the oxyanions. Their values are however notably different than those obtained by AIM.

1. Introduction

Oxyanions of the form XO_4 are of interest to a wide range of disciplines. Their binding capacities are of notable importance and have been the focus of a large number of studies.[1−3] These studies reveal important trends in the affinity of 3rd and 4th row main group oxyanions for protons and metals in aqueous solutions. Perchlorate, for instance, resists protonation in extremely acidic conditions, while the dominant species of silicate are partially protonated in alkaline solutions. The differences in charge of oxyanions, going from −1 for ClO_4^{1-} and BrO_4^{1-} to −4 for SiO_4^{4-} and GeO_4^{4-}, and the concomitant larger X−O bond lengths are obvious causes for these observations but not the only ones. The nature of X−O bonds must be also understood. In the framework of Pauling's bond valence theory,[4] each X−O bond should have a bond valence of $\nu = z/\mathrm{CN}$, where z is the formal oxidation state of X and CN = 4 is the coordination number. From this perspective, the residual charge on oxygens, $\nu - 2$, can be an indicator of the overall affinity of an oxyanion for cations, for instance. This approach has been used to determine the charge of lattice-bound oxygens at metal oxide surfaces and to partition the charge of adsorbates between Helmholtz planes in electric double-layer models.[5−6] The effects of X−O bond lengths can also be accounted for with actual bond valences.[7] This approach has notably been used to predict the affinity of aqueous monomers for protons.[8]

A more explicit treatment can be achieved with quantum-chemical calculations. Although some main-group oxyanions can be unstable in the isolated state,[9−11] it remains of interest to document their electronic structures and to compare these with systems containing stabilizing media (e.g., water) or with stable oxyanions in the isolated state. Several main-group element and transition-metal XO_4 oxyanions have been investigated by density functional methods and interpreted with molecular orbital theory and Mulliken population analyses.[12−13] The latter approach, although simple, yields notably lower atomic oxidation states than the formal expected values of X and O. The objects of this study are (1) to interpret the nature of X−O bonds in main-group XO_4 oxyanions (X = Si, P, S, Cl and Ge, As, Se, Br) and (2) to determine intramolecular charge distribution by analyzing the topology of the electron density with (1) the theory of atoms in molecules (AIM) of Bader[14] and (2) Silvi and Savin's[15] adaptation of Becke and Edgecombe's[16] electron localization function (ELF). AIM interprets bonding in terms of the properties of the "(3,−1) bond critical point", namely, the point in space where the electron density is at its minimum along a bond path[14] linking two nuclei and where it is maximum perpendicular to it. The topology of the electron density can also be used to delineate atomic basins that can in turn be integrated in terms of their electronic population. The ELF, on the other hand, quantifies the repulsion between electrons due to the Pauli exclusion principle[17] and thereby identifies regions of space where electrons are alone or present as pairs of opposite spin. These regions define basins representing either core or valence electrons, where valence electrons located between two nuclei are seen as the "pieces of glue"[18] making a chemical bond. A population analysis of these basins

* To whom correspondence should be addressed. Phone: +41 1 632 6394. Fax: +41 1 632 1088. E-mail: boily@erdw.ethz.ch.

10.1021/jp014619e CCC: $22.00
Published on Web 04/11/2002

provides an insightful view on the nature of a chemical bond and, at the same time, on the (de)localization of electrons within a molecule. Such analyses have already been carried out on perchlorate.[19] AIM and ELF electronic populations cannot, however, be condensed to point charges at the nuclei because such values do no reproduce the quantum-chemical electrostatic potentials.[20] Alternative values are presented for comparison by fitting point charges to the quantum-chemical electrostatic potential of the oxyanions with the Merz−Kollman method.[21−22]

2. Methods

2.1. Topological Analyses. *2.1.1. AIM.* AIM[14] explores the topology of the electron density, ρ, of molecules. The most revealing information is found close to planes defined by atomic centers. The electron density at the (3,−1) bond critical point, $\rho(r_c)$, that is, the point at which the electron density is at its minimum along a bond path[14] and maximum perpendicular to it, is of particular interest. The eigenvalues of the diagonalized Hessian of $\rho(r_c)$ yield one positive value parallel to a bond path ($\lambda_3 = \partial^2\rho(r_c)/\partial z^2$) and two negative values perpendicular to it ($\lambda_1 = \partial^2\rho(r_c)/\partial x^2$; $\lambda_2 = \partial^2\rho(r_c)/\partial y^2$). A chemical bond thus results from the competition of (1) the parallel expansion of ρ, which separates charges in their respective atomic basins (λ_3), and (2) the perpendicular contraction of ρ toward a bond path (λ_1,λ_2). If the former dominates, the ratios $|\lambda_1|/\lambda_3$ and $|\lambda_2|/\lambda_3$ are <1, while if the latter dominates, the ratios $|\lambda_1|/\lambda_3$ and $|\lambda_2|/\lambda_3$ are >1. The dominant effect is measured by the Laplacian of $\rho(r_c)$:

$$\nabla^2\rho(r_c) = \lambda_1 + \lambda_2 + \lambda_3 \tag{1}$$

When $\nabla^2\rho(r_c) < 0$, charge is concentrated at the critical point, while when $\nabla^2\rho(r_c) > 0$, charge is locally depleted. $\nabla^2\rho(r_c)$ takes even deeper roots by measuring the balance between the (positive) kinetic energy density, $G(r_c)$, and the (negative) electronic potential energy density, $V(r_c)$:

$$^1/_4\nabla^2\rho(r_c) = 2G(r_c) + V(r_c) \tag{2}$$

Thus, if $\nabla^2\rho(r_c)$ is large and negative, the electrons are concentrated at the bond critical point and possess a value of $V(r_c)$ that is more than twice the value of $G(r_c)$. Conversely, if $\nabla^2\rho(r_c)$ is large and positive, $G(r_c)$ is in excess. The ratio $G(r_c)/\rho(r_c)$ is also a good indicator of the average kinetic energy associated with bond critical point electrons. Typically, if $G(r_c)/\rho(r_c) > 1$, electrons possess excess kinetic energy, while if $G(r_c)/\rho(r_c) < 1$, electrons are concentrated. In summary, if bond critical points possess large values of $\rho(r_c)$ and $-\nabla^2\rho(r_c)$ and values of $G(r_c)/\rho(r_c) < 1$, $|\lambda_1|/\lambda_3 > 1$, and $|\lambda_2|/\lambda_3 > 1$, electrons are locally concentrated and result in a "shared interaction" (covalent, dative, metallic bonds) of electrons between two atomic centers, as envisioned by Lewis.[23−24] Conversely, if bond critical points possess small values of $\rho(r_c)$ and large values of $\nabla^2\rho(r_c)$ and values of $G(r_c)/\rho(r_c) > 1$, $|\lambda_1|/\lambda_3 < 1$, and $|\lambda_2|/\lambda_3 < 1$, electrons are not concentrated at this point and tend to separate in their respective atomic basins resulting in a "closed-shell interaction" (ionic, hydrogen, van der Waals bonds). Finally, the local electronic energy density, $E_e(r_c)$, adds further insight on the stability of an interaction:

$$E_e(r_c) = G(r_c) + V(r_c) \tag{3}$$

where values of $E_e(r_c) < 0$ are indicative of a stabilizing accumulation of charge.

2.1.2. ELF. The ELF approach consists of quantifying the electron density in the whole molecular space in terms of the normalized local excess kinetic energy of electrons due to the Pauli exclusion principle:[16−17]

$$\eta(r) = \frac{1}{1 + \left(\frac{D_\sigma(r)}{D_\sigma^0(r)}\right)^2} \tag{4}$$

where $D_\sigma(r)$ is the local excess kinetic energy density due to Pauli repulsion and makes use of a single determinental wave function built from Hartree−Fock or Kohn−Sham orbitals, and D_σ is the a reference homogeneous electron gas of the same density, which acts as a renormalization factor. Thus, a value of $\eta(r) = 0.5$ corresponds to a homogeneous electron gas, whereas larger values, up to a maximum of $\eta(r) = 1.0$, correspond to larger probabilities of finding electrons alone or in pairs of antiparallel spins in a given region of space. The gradient field of the ELF is used to partition space into basins.[15] Basins can represent core or valence electrons, denoted as C(X) and V(X,...) for atom X, respectively.[25] Valence basins are categorized according to their synaptic order, namely, the number of core basins with which they share a common boundary. A monosynaptic valence basin, V(X), encompasses nonbonding electrons while di- or polysynaptic valence basins, $V(X,O_1,...,O_n)$, encompass electrons involved in bi- or multicentric bonds. The presence of di- or polysynaptic basins is thus indicative of shared interactions (covalent, dative, metallic bonds), while the absence of these basins is indicative of closed-shell interactions (ionic, hydrogen, van der Waals bonds), provided that the atoms are indeed bound. Synaptic basins can be visualized for any given range of isodensity values of $\eta(r) = f$, which in turn enclose regions of $\eta(r) \geq f$.

The electronic population of a synaptic basin, $\bar{N}$, is obtained as the integral of the one-electron density over the basin. The variance of the basin population, $\sigma^2(\bar{N})$, represents the quantum-mechanical uncertainty of the basin population and is a result of the delocalization of electrons.[18] It is also written as the sum of the contributions of all other basins and is used as a normalization factor to represent the cross-contribution between two specific basins on a percentage basis,[18] a quantity that will here only be alluded to on a qualitative basis. Last, the relative fluctuation of a basin[14] can be expressed as

$$\lambda = \sigma^2(\bar{N})/\bar{N} \tag{5}$$

namely, the variance of the basin normalized for the electronic population. This will be used to describe the degree of delocalization, where values above 0.45 denote delocalized electrons.[25]

2.2. Computational Details. Geometries of all XO_4 oxyanions were fully optimized with the MP2(full)[26] and the B3LYP methods[27,28] using the Cartesian 6-311+G(d) and 6-311+G(3df) basis sets.[29] Wave functions obtained as *wfn* files were generated at the B3LYP level with the Cartesian 6-311+G(3df) basis set with a tight convergence criterion.[29] The stability of the single-determinant wave functions[30,31] and frequency calculations were furthermore tested for each oxyanion. Last, atomic charges were fitted on the electrostatic potential of each oxyanion with the Merz−Kollman[21,22]method on 10 layers with 300 points per Å^3 (i.e., about 50 000 points in total). The default van der Waals radii of Gaussian 98[29] were taken as such, except for Ge (2.25 Å), As (2.00 Å), and Se (2.00 Å). All calculations were carried out with Gaussian 98.[29]

TABLE 1: X−O Bond Lengths (Å)

	B3LYP		MP2=full	
	6-311+G(d)	6-311+G(3df)	6-311+G(3df)	experiment
ClO_4^{1-}	1.501	1.458	1.457	1.431−1.457[38−39]
SO_4^{2-}	1.527	1.502	1.505	1.464−1.552[40−49]
PO_4^{3-}	1.603	1.588	1.592	1.497−1.604[50−61]
SiO_4^{4-}	1.721	1.701	1.707	1.595−1.640[62−67]
BrO_4^{1-}	1.654	1.630	1.607	1.60−1.62[39,68]
SeO_4^{2-}	1.691	1.667	1.669	1.635−1.65[39,69−70]
AsO_4^{3-}	1.750	1.739	1.746	1.654−1.69[71−73]
GeO_4^{4-}	1.836	1.811	1.813	1.747−1.89[74−80]

The *wfn* files are used for topological analyses of the electron density in the frameworks of AIM with the program MORPHY98[32] and of ELF with the program TopMoD.[33] MORPHY98 is used to localize (3,−1) critical points of X−O bonds,[34−35] to characterize these in terms of (1) $\rho(r_c)$, (2) λ_1, λ_2, λ_3, (3) $\nabla^2\rho(r_c)$, and (4) $G(r_c)$,[14] and to calculate the electronic population of the atomic basins.[36−37] TopMoD is used to identify synaptic basins[15,18] and to obtain correlative values of $\bar{N}$, $\sigma^2(N)$, and λ on a working grid of 0.1 au. Visual representations of the synaptic basins are obtained at a resolution of 0.4 au.

3. Results and Discussion

3.1. Geometry Optimization. Geometry optimization calculations give support to T_d symmetry for all of the oxyanions considered in this study, except for GeO_4^{4-}. Frequency calculations of GeO_4^{4-} with a forced T_d symmetry yield two imaginary frequencies, while the fully optimized GeO_4^{4-} with a distorted geometry only yields real frequencies. Frequency calculations also confirmed the optimal geometries of all other oxyanions to correspond to the energy minima. The stability of single determinant wave functions[30,31] was confirmed for all oxyanions at the B3LYP/6-311+G(3df) level, except for GeO_4^{4-} and SiO_4^{4-}. Topological analyses of ρ were nonetheless carried out on these oxyanions for comparative purposes.

All calculations at the 6-311+G(3df) basis set give bond lengths close to experimental values of solid oxyanions[38−80] (Table 1), with increasing deviation for oxyanions of larger charge. This discrepancy results from the larger charge difference between free oxyanion molecules and those of the solid bulk, where charge is neutralized. B3LYP calculations with fewer polarization functions or with basis sets of double-ζ quality (cf. ref 12) or both tend to overestimate bond lengths. The wave functions used to analyze the topology of the electron density of oxyanions were therefore generated with the Cartesian 6-311+G(3df) basis set, using the B3LYP method.

3.2. AIM Bonding Analysis. The properties of the electron density at the (3,−1) bond critical points are reported in Table 2. All values of $\rho(r_c)$ suggest significant concentrations of electrons at the bond critical point, with values decreasing across Cl through Si and Br through Ge oxyanions. Furthermore, because $\lambda_1 = \lambda_2$, these electrons spread symmetrically on the two planes perpendicular to the bond path. The ellipticity[14] of the bond is then said to be zero, suggesting the absence of π bonding in these oxyanions. The bond critical point electrons (shown as solid squares in Figure 1) of most oxyanions are in regions of positive values of $\nabla^2\rho(r_c)$ and therefore possess an excess (positive) local kinetic energy density, $G(r_c)$ (eq 2). The values of $G(r_c)/\rho(r_c) > 1$ furthermore support this concept, with decreasing values across both series down to exceptionally $G(r_c)/\rho(r_c) < 1$ for ClO_4^{1-} and BrO_4^{1-}. The ratios $|\lambda_1|/\lambda_3$ and $|\lambda_2|/\lambda_3$ are all well below the nominal value of 1, except for ClO_4^{1-} and BrO_4^{1-}, which results from the parallel expansion of ρ away from the interatomic surface. Given the relatively large values of $\rho(r_c)$, this separation of charge is however not fully characteristic of closed-shell interactions. Rather, the X−O bonds are best seen as intermediate to closed-shell and shared interactions with (1) an increasing degree of shared interactions going from SiO_4^{4-} to ClO_4^{1-} and from GeO_4^{4-} to BrO_4^{1-}, (2) ClO_4^{1-} as the only oxyanion exhibiting true shared interactions, and (3) BrO_4^{1-} at the threshold of a truly closed-shell interaction. This is also well-illustrated in Figure 1, especially for 3rd row oxyanions, where the contour lines of negative values of $\nabla^2\rho$ progressively encompass the molecule, rather than separate atoms. Values of $E_e(r_c)$ also show that the accumulation of charge at the bond critical points tends to be stable.

TABLE 2: AIM Analysis at the B3LYP/6-311+G(3df) Level

	$\rho(r_c)^a$	$\nabla^2\rho(r_c)^b$	$\lambda_1/\lambda_3{}^c$	$G(\rho(r_c))/\rho(r_c)^d$	$E_e(r_c)^e$
ClO_4^{1-}	0.37	−0.93	1.61	0.90	−0.71
SO_4^{2-}	0.28	0.14	0.44	1.37	−0.33
PO_4^{3-}	0.19	0.57	0.27	1.54	−0.06
SiO_4^{4-}	0.12	0.61	0.21	1.62	0.05
BrO_4^{1-}	0.27	−0.01	0.51	0.98	−0.27
SeO_4^{2-}	0.22	0.20	0.39	1.11	−0.16
AsO_4^{3-}	0.18	0.38	0.29	1.22	−0.07
GeO_4^{4-}	0.14	0.47	0.23	1.31	−0.06

[a] Electron density in au. [b] Laplacian of the electron density (eq 1) in au. [c] Ratio of the eigenvalues of the Hessian of $\rho(r_c)$ perpendicular ($\lambda_1 = \lambda_2$) and parallel (λ_3) to the X−O bond path in au. [d] Ratio of the electronic kinetic energy density and the electron density in au. [e] Electronic energy density (eq 3) in au.

The Laplacian of ρ also recovers four "(3,−3) critical points"[14] in each oxygen valence shell. These are points where the eigenvalues of the diagonalized Hessian of $\nabla^2\rho$ indicate a maximum from all approaches, namely, a concentration of charge. One of these points is located along the bond path between X and O, corresponding to a local concentration of bonding electrons. The three other points are invariably located at 0.35 Å from the nucleus of O and are diametrically opposite to the X−O axis, that is, pointing toward the surface of the molecule. Electrons located around these critical points can be seen as part of three nonbonding electron pairs, further suggesting the absence of π bonding in these molecules. They also obey C_{3v} symmetry about an axis defined by X−O. The dihedral between a plane formed by two (3,−3) critical points and the O nucleus and a vector formed by the third critical point and the O nucleus ranges from 143° for ClO_4^{1-} to 127° for SiO_4^{4-} and from 152° for BrO_4^{1-} to 143° for GeO_4^{4-}. The centers of the regions occupied by nonbonded electron pairs are thus closer together for oxyanions of larger charge, but this has no direct inference on the volumes occupied by these electrons.

3.3. ELF Bonding Analysis. Figure 2 shows typical localization domains of the oxyanions. All but GeO_4^{4-} possess the same 21 ELF basins, namely, five monosynaptic core basins, C(X) and C(O), four disynaptic valence basins, V(X,O), and 12 monosynaptic basins representing O valence electrons pairs, V(O). GeO_4^{4-} does not formally possess disynaptic basins but has the 17 other basins. Visual representations of 3rd row oxyanions are typical of Figure 2a with the clear presence of V(X,O) basins. Each O has the three V(O) basins merged to form a pierced sphere oriented toward C(X) and with the most localized electrons forming a torus the plane of which is roughly perpendicular to the X−O axis. Fourth row oxyanions are strikingly different with the notable absence of V(X,O) basins at any values of $\eta(r)$ and with three merged V(O) basins surrounding C(O) in a sphere-like fashion but polarized toward C(X). The a priori interpretation would thus classify 3rd row

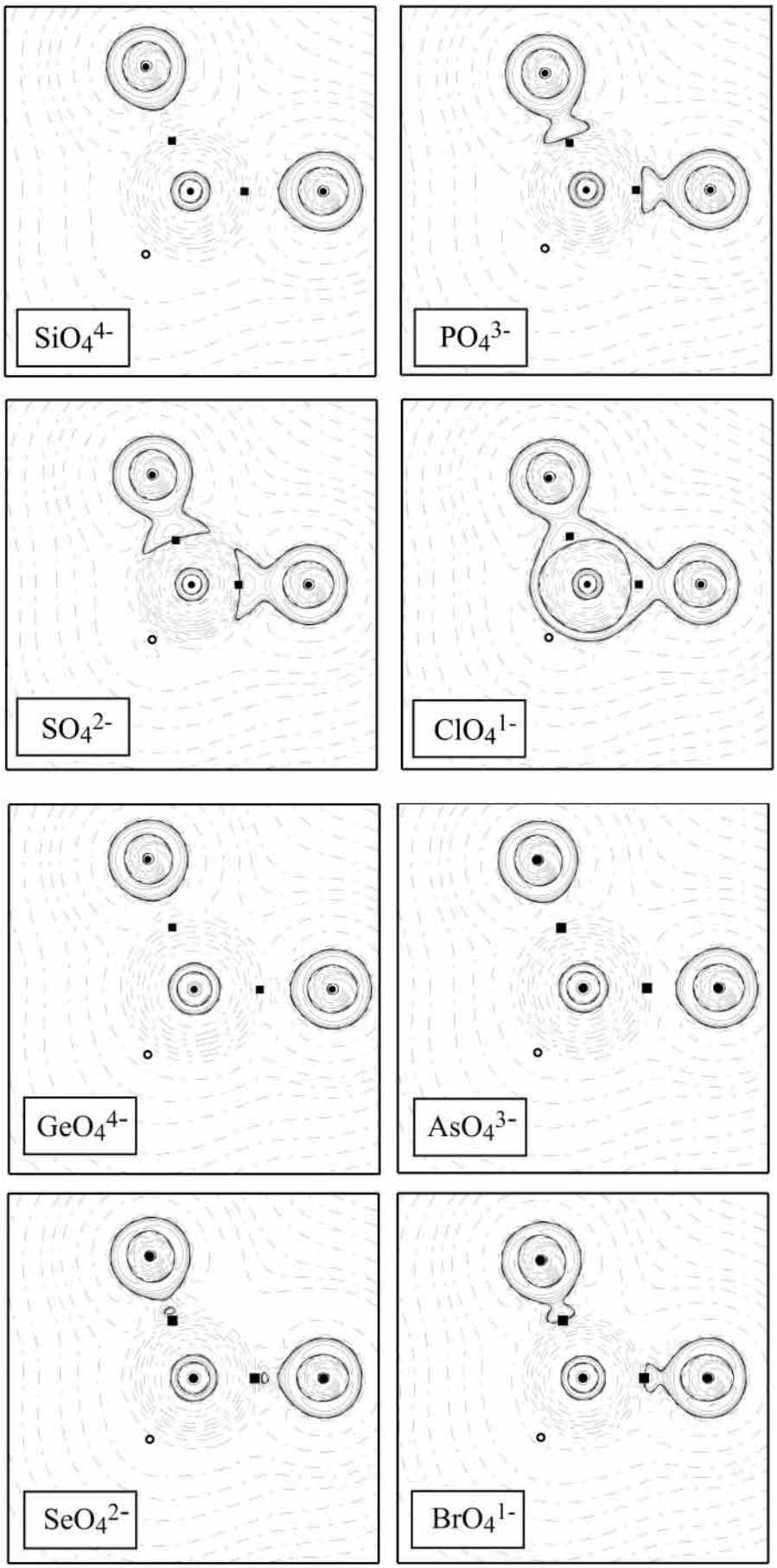

Figure 1. Contour maps of the Laplacian of the electron density, $\nabla^2\rho$, at a plane defined by the nuclei of X and of two O. Solid squares show the positions of the (3,−1) bond critical points in ρ. Solid lines represent negative values and dashed lines positive values. Small open circles represent out-of-plane oxygens. Maps were produced with MORPHY98[32] from Gaussian 98[29] *wfn* files generated at the B3LYP/6-311+G(3df) level.

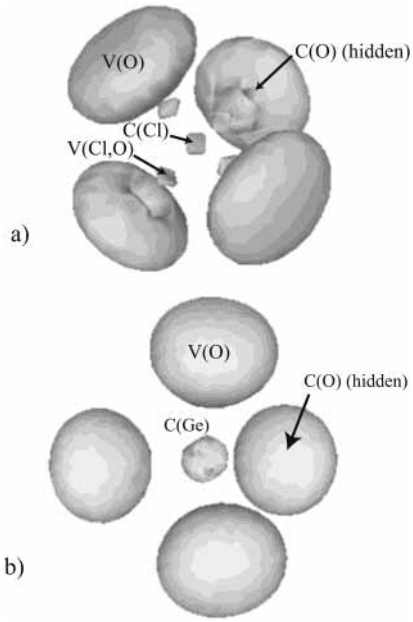

Figure 2. Electron localization basins determined by ELF for (a) ClO_4^{1-} and (b) GeO_4^{4-} both at an isodensity of $\eta = 0.74$ produced with TopMod[33] at a grid step of 0.4 au from Gaussian 98[29]*wfn* files generated at the B3LYP/6-311+G(3df) level. All V(O) basins are of identical volume but do not appear as such due to perspective effects.

oxyanions as characteristic of shared interactions and 4th row oxyanions as mostly of closed-shell interactions.

The results of Table 3 show the core populations of 3rd row element oxyanions to be highly localized with $\lambda = 0.04-0.06$ and with $\bar{N} = 10.02-10.05e$, as expected for the L-shell. The excess of $0.02-0.05e$ is ascribed to some mixing of some valence shell electrons to the core.[18] Those of the 4th row elements are also highly localized, with $\lambda = 0.04$ but with $0.15-0.22e$ less than the expected value from the electronic configuration [X] = [Ar $3d^{10}$] of $28e$. This phenomenon has been tentatively ascribed to some mixing of 3d electrons in the valence shell.[81] The populations of all core oxygens are invariably at $2.05-2.07e$ and are highly localized with $\lambda = 0.17$. The more significant differences between oxyanions are found in the valence shell electrons. All disynaptic basins V(X,O) have electron populations that are lower than the $2e$ of Lewis[23,24] with values ranging from $1.56e$ (SiO_4^{4-}) to $1.84e$ (ClO_4^{1-}) and from $0e$ (GeO_4^{4-}) to $0.30e$ (BrO_4^{1-}). These electrons are furthermore highly delocalized with $\lambda = 0.67$ for 3rd row and $\lambda = 0.90$ for 4th row oxyanions and exhibit strong cross-contributions with V(O). Each O has three V(O) basins containing roughly $2e$ the centers of which are all invariably at 0.58 Å from the nucleus and only 0.23 Å from (3,−3) $\nabla^2\rho$ critical points of AIM. The strong delocalization ($\lambda > 0.5$) and strong cross-contributions[18] of these three ELF basins (not shown) provide justification to merge these into one superbasin of about six to eight electrons that are in this context seen as localized ($\lambda = 0.17-0.24$). The population of these basins depends on the nature of the X−O bonds. Monosynaptic electron populations of 3rd row oxyanions range from $6.12e$ to $6.39e$, that is, close to Lewis' three electron pairs, and those of 4th row oxyanions range from $7.69e$ to $7.99e$, that is, close to Lewis' four electron pairs.

Third row X−O bonds are characteristic of polarized shared interactions with the center of disynaptic basins closer to O than X in the order Si > P > S > Cl, as expected from the differences in electronegativities. ELF results at various bond lengths (Figure 3) provide additional information.[82] The electron population of the V(Cl,O) basin, shown in Figure 3a, decreases from $1.84e$ at 1.46 Å to $1.64e$ at the threshold of the Cl−O bond break (1.59−1.71 Å), while that of each of the three V(O) basins increases accordingly from $2.04e$ to $2.10e$ This phenomenon is also recovered from the original ELF results from SiO_4^{4-} to ClO_4^{1-}, with the only exception that the smaller nucleic charges of Si, P, and S result in smaller V(X,O) populations than that of V(Cl,O). A catastrophe[82] occurs between 1.59 and 1.71 Å with the replacement of the V(Cl,O) basin with V(Cl). The electron population of V(Cl) ranges from $1.62e$ (1.71 Å) to $1.64e$ (2.00 Å), with that of V(O) converging toward oxygens' nominal six valence electrons. The transformation of the synaptic order of a basin during bond breaking is known as a *tautomorphic diffeosynaptic*[82] process and is indicative of a donor−acceptor type Cl−O (dative) bond, as shown in ref 19.

The disynaptic population of fourth row oxyanions is not only nearly insignificant (about $0.3e$) but is also highly delocalized with strong cross-contributions with the V(O) basins. ELF results at various Br−O bond lengths (Figure 3b) show essentially the same features as ClO_4^{1-} but on a more dramatic scale. The V(Br,O) population increases from $0.27e$ at 1.61 Å to $0.40e$ at 1.67 Å. The basin is then replaced by V(Br), a monosynaptic basin representing valence electrons of Br, the population of which subsequently increases to $1.63e$ at 2.00 Å. Once more, this is a tautomorphic diffeosynaptic process with the only difference that the population of the new V(Br) basin increases dramatically from about $0.4e$ to $1.37e$ to reach similar values as those of V(Cl) at X−O bond lengths greater than 1.8 Å. Last, the variations in the V(O) populations are consequences of the changes in V(Br,O)/V(Br) and also converge to their nominal $2e$ at great X−O bond lengths. From this analysis, the weak shared interactions in Br−O can be seen as dative but the more important bonding process is of closed-shell nature.

3.4 Intramolecular Charge Distribution. AIM and ELF can provide information on the statistical distribution of electrons within a molecule. The increase in the negative charge on O from ClO_4^{1-} to SiO_4^{4-} and from BrO_4^{1-} to GeO_4^{4-}, ascribed to the transfer of charge from the disynaptic V(X,O) to the monosynaptic V(O) basin, is also recovered by the integration results of the atomic basins defined by AIM (Table 4). Indeed, as the degree of shared interactions in the X−O bond lessens, O tends to gain its four electron pairs and consequently the net AIM charge converges toward its formal value of −2. However, given the large values of $\rho(r_c)$, AIM integrations necessarily ascribe electrons to the valence shell of X and therefore intrinsically imply a lower oxidation state, noting also that the electrons do possess a local excess of kinetic energy. It is furthermore noteworthy to mention that although the same conclusions can be reached with a Mulliken population analysis[9] (also Table 4) AIM remains more reliable given its more rigorous definition of atomic basins and its relative insensitivity to the choice of basis sets.[20]

Notwithstanding the explicit notion of intraatomic electron distributions in AIM and ELF, long-range electrostatic potentials cannot be reproduced if these charges are condensed to point charges.[20] The Merz−Kollman scheme was therefore used to fit point charges located at the atomic nuclei with the electrostatic potential. The results, shown in Table 4, are indeed significantly different than those of AIM and Mulliken population analyses.

4. Conclusions

The concepts of AIM and ELF tend to concord on the nature of the X−O bond of 3rd and 4th row main-group element

TABLE 3: ELF Analysis at the B3LYP/6-311+G(3df) Level

	basin	$\bar{N}^a$	$\sigma^2(\bar{N})^b$	$\lambda(\bar{N})^c$		basin	$\bar{N}^a$	$\sigma^2(\bar{N})^b$	$\lambda(\bar{N})^c$
ClO_4^{1-}	C(Cl)	10.02	0.59	0.06	BrO_4^{1-}	C(Br)	27.78	1.19	0.04
	C(O)	2.06	0.34	0.17		C(O)	2.05	0.34	0.17
	V(Cl,O)	1.84	1.21	0.67		V(Br,O)	0.30	0.27	0.90
	V(O)	6.12	1.25	0.24		V(O)	7.69	1.56	0.20
SO_4^{2-}	C(S)	10.02	0.53	0.05	SeO_4^{2-}	C(Se)	27.81	1.10	0.04
	C(O)	2.06	0.35	0.17		C(O)	2.06	0.34	0.17
	V(S,O)	1.77	0.49	0.67		V(Se,O)	0.28	0.23	0.89
	V(O)	6.16	1.44	0.23		V(O)	7.67	1.44	0.19
PO_4^{3-}	C(P)	10.03	0.48	0.05	AsO_4^{3-}	C(As)	27.85	1.04	0.04
	C(O)	2.07	0.35	0.17		C(O)	2.06	0.34	0.17
	V(P,O)	1.61	1.08	0.66		V(As,O)	0.27	0.25	0.90
	V(O)	6.30	1.42	0.22		V(O)	7.69	1.37	0.18
SiO_4^{4-}	C(Si)	10.05	0.40	0.04	GeO_4^{4-}	C(Ge)	27.80	0.97	0.04
	C(O)	2.07	0.35	0.17		C(O)	2.06	0.34	0.17
	V(Si,O)	1.56	1.04	0.67		V(O)	7.99	1.33	0.17
	V(O)	6.39	1.44	0.23					

[a] Electronic population (*e*). [b] Variance of $\bar{N}$. [c] Relative fluctuation of $\bar{N}$.

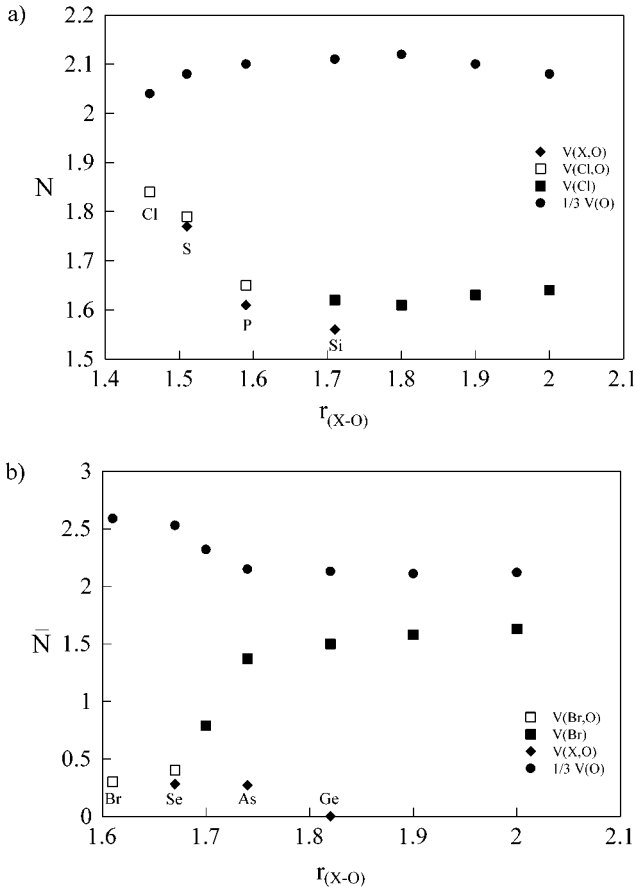

Figure 3. ELF analysis of (a) ClO_4^{1-} and (b) BrO_4^{1-} for different Cl−O and Br−O bond lengths, respectively. The V(O) basins are those of (a) ClO_4^{1-} and (b) BrO_4^{1-}. The populations of the disynaptic basins of the other XO_4 oxyanions are also shown as diamonds but not those of their correlative V(O) basins.

oxyanions. AIM analyses suggest that perchlorate is the only oxyanion with true shared interactions while all others are intermediate to shared and closed-shell interactions with increasing character for the latter in the series Si through Cl and Ge through Br. The ELF supports this for 3rd row oxyanions with a disynaptic basin population of 1.57*e* for SiO_4^{4-} increasing to 1.86*e* for ClO_4^{1-}. Fourth row oxyanions, with disynaptic basin populations ranging from 0 for GeO_4^{4-} to 0.30 for BrO_4^{1-} are however in large part of closed-shell character. It should also

TABLE 4: Atomic Charges (*e*) at the B3LYP/6-311+G(3df) Level

	AIM[a]		Mulliken		MK[b]	
	X	O	X	O	X	O
ClO_4^{1-}	3.05	−1.01	1.54	−0.64	0.98	−0.50
SO_4^{2-}	3.58	−1.39	1.33	−0.83	1.59	−0.89
PO_4^{3-}	3.62	−1.65	1.66	−1.16	2.36	−1.34
SiO_4^{4-}	3.09	−1.77	3.23	−1.81	4.64	−2.16
BrO_4^{1-}	2.77	−0.94	1.9	−0.73	0.62	−0.41
SeO_4^{2-}	2.85	−1.21	1.77	−0.94	1.18	−0.79
AsO_4^{3-}	3.65	−1.41	1.43	−1.11	1.53	−1.13
GeO_4^{4-}	4.29	−1.57	4.07	−2.01	1.34	−0.67

[a] The error on the integration of the AIM atomic basin is less than 0.01*e*. [b] Merz−Kollman method with 300 points/Å^3 on 10 levels.

be noted that while AIM analyses of SiO_4^{4-} and GeO_4^{4-} are similar, those of ELF yield markedly contrasting interpretations. Otherwise, both approaches are rather complementary to one another.

ELF analyses have also shown the V(O) populations to be larger for oxyanions with stronger closed-shell character. Such oxyanions therefore tend to have four electron pairs localized in the valence shell of each oxygen, a result that is also recovered in the analysis of the Hessian of $\nabla^2\rho$. The atomic oxidation state obtained by AIM furthermore suggests values lower than the formal values. Last, point charges optimized according to the Merz−Kollman scheme can reproduce the electrostatic potential of the oxyanions with, however, notably different values of the AIM atomic charges.

Acknowledgment. This work was supported by the Swiss Federal Institute of Technology (ETH), Zürich. The Competence Centre for Computational Chemistry (C4) at ETH is thanked for providing access and support to its facilities. O. Suleimenov is thanked for his useful advice throughout the course of this study, and B. Silvi is also thanked for his invaluable help with TopMoD.

References and Notes

(1) Smith, R. M.; Martell, A. E. *Critical Stability Constants. Volume 4: Inorganic Complexes*; Plenum Press: New York, 1976.

(2) Martell, A. E.; Smith, R. M. *Critical Stability Constants. Volume 5: First Supplement*; Plenum Press: New York, 1982.

(3) Martell, A. E.; Smith, R. M. *Critical Stability Constants. Volume 6: Second Supplement*; Plenum Press: New York, 1989.

(4) Pauling, L. *J. Am. Chem. Soc.* **1929**, *51*, 1010.

(5) Hiemstra, T.; Venema, P.; van Riemsdijk, W. H. *J. Colloid Interface Sci.* **1996**, *184*, 680.
(6) Rietra, R. P. J. J.; Hiemstra, T.; van Riemsdijk, W. H. *Geochim. Cosmochim. Acta* **1999**, *63*, 3009.
(7) Brown, I. D.; Altermatt, D. *Acta Crystallogr. B* **1985**, *41*, 244.
(8) Hiemstra, T.; Venema, P.; van Riemsdijk, W. H. *J. Colloid Interface Sci.* **1996**, *184*, 680.
(9) Bridgeman, A. J.; Cavigliasso, G. *Polyhedron* **2001**, *20*, 2269.
(10) Stückl, A. C.; Daul, C. A.; Güdel, H. U. *J. Chem. Phys.* **1997**, *107*, 4606.
(11) Boldyrev, A. I.; Simons, J. *J. Phys. Chem.* **1994**, *98*, 2298.
(12) Stefanovich, E. V.; Boldyrev, A. I.; Truong, T. N.; Simons, J. *J. Phys. Chem. B* **1998**, *102*, 4205.
(13) Wang, X.-B.; Nicholas, J. B.; Wang, L.-S. *J. Chem. Phys.* **2000**, *113*, 10837.
(14) Bader, R. F. W. *Atoms In Molecules: A Quantum Theory*; Clarendon Press: Oxford, U.K., 1990.
(15) Silvi, B.; Savin, A. *Nature* **1994**, *371*, 683.
(16) Becke, A. D.; Edgecombe, K. E. *J. Chem. Phys.* **1990**, *92*, 5397.
(17) Savin, A.; Jepsen, O.; Flad, J.; Andersen, O. K.; Preuss, H.; von Schnering, J. G. *Angew. Chem., Int. Ed. Engl.* **1992**, *31*, 187.
(18) Noury, S.; Colonna, N.; Savin, A.; Silvi, B. *J. Mol. Struct.* **1998**, *450*, 59.
(19) Beltrán, A.; Andrés, J.; Noury, S.; Silvi, B. *J. Phys. Chem. A* **1999,** *103*, 3078.
(20) Sigfridsson, E.; Ryde, U. *J. Comput. Chem.* **1998**, *19*, 377.
(21) Sing, U. C.; Kollman, P. A. *J. Comput. Chem.* **1984**, *5*, 129.
(22) Besler, B. H.; Merz, K. M.; Kollman, P. A. *J. Comput. Chem.* **1990**, *11*, 431
(23) Lewis, G. N. *J. Am. Chem.. Soc.* **1916**, *38*, 762.
(24) Lewis, G. N. *J. Chem. Phys.* **1933**, *1*, 17.
(25) Savin, A.; Silvi, S.; Colonna, F. *Can. J. Chem.* **1996**, *74*, 1088.
(26) Møller, C.; Plesset, M. S. *Phys. Rev.* **1934**, *46*, 618.
(27) Lee, C.; Yang, W.; Parr, R. G. *Phys. Rev. B* **1988**, *37*, 785.
(28) Becke, A. D. *J. Chem. Phys.* **1993**, *98*, 5648.
(29) Frisch, M. J.; Trucks, G. W.; Schlegel, H. B.; Scuseria, G. E.; Robb, M. A.; Cheeseman, J. R.; Zakrzewski, V. G.; Montgomery, J. A., Jr.; Stratmann, R. E.; Burant, J. C.; Dapprich, S.; Millam, J. M.; Daniels, A. D.; Kudin, K. N.; Strain, M. C.; Farkas, O.; Tomasi, J.; Barone, V.; Cossi, M.; Cammi, R.; Mennucci, B.; Pomelli, C.; Adamo, C.; Clifford, S.; Ochterski, J.; Petersson, G. A.; Ayala, P. Y.; Cui, Q.; Morokuma, K.; Malick, D. K.; Rabuck, A. D.; Raghavachari, K.; Foresman, J. B.; Cioslowski, J.; Ortiz, J. V.; Stefanov, B. B.; Liu, G.; Liashenko, A.; Piskorz, P.; Komaromi, I.; Gomperts, R.; Martin, R. L.; Fox, D. J.; Keith, T.; Al-Laham, M. A.; Peng, C. Y.; Nanayakkara, A.; Gonzalez, C.; Challacombe, M.; Gill, P. M. W.; Johnson, B. G.; Chen, W.; Wong, M. W.; Andres, J. L.; Head-Gordon, M.; Replogle, E. S.; Pople, J. A. *Gaussian 98*, revision A.9; Gaussian, Inc.: Pittsburgh, PA, 1998.
(30) Seeger, R.; Pople, J. A. *Chem. Phys.* **1977**, *66*, 3045.
(31) Bauernschmitt, R.; Ahlrichs, R. *J. Chem. Phys.* **1996**, *104*, 9047.
(32) MORPHY98 is a program written by P. L. A. Popelier with a contribution from R. G. A. Bone, UMIST, Manchester, England, EU, 1998.
(33) Noury, S.; Krokidis, X.; Fuster, F.; Silvi, B. *Comput. Chem.* **1999**, *23*, 597.
(34) Popelier, P. L. A. *Chem. Phys. Lett.* **1994**, *228*, 160.
(35) Popelier, P. L. A. *Comput. Phys. Commun.* **1996**, *93*, 212.
(36) Popelier, P. L. A. *Mol. Phys.* **1996**, *87*, 1169.
(37) Popelier, P. L. A. *Comput. Phys. Commun.* **1998**, *108*, 180.
(38) Olovsson, I. *J. Chem. Phys.* **1968**, *49*, 106.
(39) Kálmán, A. *J. Chem. Soc. A* **1971**, *Part II*, 1857.
(40) Alcock, N. W.; Evans, D. A.; Jenkins H. D. B. *Acta Crystallogr. B* **1982**, *24*, 1968.
(41) Weber, H. J.; Schulz, M.; Schmitz, S.; Granzin, J.; Siegert, H. *J. Phys.: Condens. Matter* **1989,** 8543.
(42) Hill, R. J. *Can. Mineral.* **1977,** *15,* 522.
(43) Mehrotra, B. N. *Z. Kristallogr.* **1981**, *155*, 159.
(44) Moodenbaugh, A. R.; Hartt J. E.; Hurst J. J.; Youngblood R. W.; Cox D. E.; Frazer B. C. *Phys. Rev. B: Condens. Matter Mater. Phys.* **1983** *28*, 3501.
(45) Sawada, H.; Takeuchi, Y. *Z. Kristallogr.* **1990**, *191*, 167.
(46) Mentzen, B. F.; Latrach, A.; Bouix, J.; Hewat, A. W. *Mater. Res. Bull.* **1984**, *19*, 549.
(47) Coing-Boyat, J. *C. R. Hebd. Séances ′Acad. Sci.* **1962,** *255*, 1962.
(48) Hawthorne, F. C.; Ferguson, R. B. *Can. Mineral.* **1975**, *13*, 289.
(49) Rasmussen, S. E.; Jörgensen, J.-E.; Lundtoft, B. *J. Appl. Crystallogr.* **1996**, *29*, 42.
(50) Dickens, B.; Prince, E.; Schroeder, L. W.; Jorden, T. H. *Acta Crystallogr.* **1974**, *30*, 1470.
(51) Goiffon, A.; Bayle, G.; Astier, R.; Jumas, J. C.; Maurin, M.; Phillipot, E. *Rev. Chim. Minér.* **1983**, *20*, 338.
(52) Sowa, H.; Macave, J.; Schulz, H. *Z. Kristallogr.* **1990**, *192*, 119.
(53) Milligan, W. O.; Mullica, D. F. *Acta Crystallogr. C* **1983**, *39*, 23.
(54) Deschizeaux-Cheruy, M. N.; Aubert, J. J.; Joubert, J. C.; Capponi, J. J.; Vincent, H. *Solid State Ionics* **1982,** *7*, 171.
(55) Poojary, D. M.; Borade, R. B.; Clearfield, A. *Inorg. Chim. Acta* **1993**, *208*, 23.
(56) Simmen, A.; McCusker, L. B.; Baerlocher, C.; Meier, W. M. *Zeolites* **1991**, *11*, 654.
(57) Kiat, J. M.; Yamada, Y.; Chevriert, G.; Uesu, Y.; Boutrouille, P.; Calvarin, G. *J. Phys.: Condens. Matter* **1992**, *4*, 4915.
(58) Kurbanov, K. M. *Kristallografiya* **1987**, *32*, 1265.
(59) Sowa, H. *Z. Kristallogr.* **1994**, *209*, 954.
(60) Rasmussen, S. E.; Jörgensen, J.-E.; Lundtoft, B. *Powder Diffr.* **1993**, *8*, 164.
(61) Ni, Y.-X.; Hughes, J. M.; Mariano, A. N. *Am. Mineral.* **1995**, *80*, 21.
(62) Wright, A. E.; Lehmann, M. S. *J. Solid State Chem.* **1981**, *36*, 371.
(63) Smith, G. S.; Alexander, L. E. *Acta Crystallogr.* **1963** *16*, 4.
(64) Levien, L.; Prewitt, C. T.; Weidner, D. J. *J. Am. Miner.* **1980**, *65*, 920.
(65) Jörgensen, J. D. *J. Appl. Phys.* **1978**, *49*, 5473.
(66) Siggel, A.; Jansen, Z. *Anorg. Allg. Chem.* **1990**, *583*, 67.
(67) Furhmann, J.; Pickardt, J. *Anorg. Allg. Chem.* **1986**, *532*, 171.
(68) Roegner, P.; Schiessl, U.; Range, K.-J. *Z. Naturforsch.* **1993**, *B48*, 235.
(69) Yamada, N.; Ikeda, T. *J. Phys. Soc. Jpn.* **1984**, *53*, 2555.
(70) Fábry, J.; Breczewski, T.; Petříček, V. *Acta Crstallogr. B* **1979**, *35*, 588.
(71) Schaefer, W. P.; Will, G.; Mueller-Vogt, G. *Acta Crystallogr. B* **1979**, *35*, 588.
(72) Lohmueller, G.; Schmidt, G.; Deppisch, B.; Gramlich, V.; Scheringer C. *Acta Crystallogr. B* **1973**, *29*, 141.
(73) Effenberger, H. *Z. Kristallogr.* **1998**, *213*, 42.
(74) Morimoto, N.; Akimoto, S. I.; Koto, K.; Tokonami, M. *Science* **1969**, *165*, 586.
(75) Durif, A.; Averbuch-Pouchot, M. T. *C. R. Séances ′Acad. Sci., Sér. C* **1982**, *295*, 555.
(76) Hegenbart, W.; Rau, F.; Range, K. J. *Mater. Res. Bull.* **1981**, *16*, 413.
(77) Radaev, S. F.; Muradyan, L. A.; Kargin, Yu. F.; Sarin, V. A.; Kanepit, V. N.; Simonov, V. I. *Kristallografiya* **1990**, *35*, 361.
(78) Ennaciri, A.; Michel, D.; Perez y Jorba, M.; Pannetier, J. *Mater. Res. Bull.* **1984**, *19*, 793
(79) Ennaciri, A.; Kahn, A.; Michel, D. *J. Less-Common Met.* **1986**, *124*, 105.
(80) Colbeau-Justin, C.; Walez, G.; Elfakir, A.; Quarton, M.; Suard, E. *J. Solid State Chem.* **1997**, *134*, 59.
(81) Berski, S.; Silvi, B.; Latajka, Z.; Leszczynski, J. *J. Chem. Phys.* **1999**, *111*, 2542.
(82) Krokidis, X.; Noury, S.; Silvi, B. *J. Phys. Chem. A* **1997**, *101*, 7277.